INTERPRETING THERMOCOUPLE READING IN FUEL ASSEMBLY HEAD - A CFD STUDY ON COOLANT MIXING

Karoliina Myllymäki, Timo Toppila, Tellervo Brandt

Fortum Nuclear Services Ltd, P.O.B. 100, FI-00048 Fortum, Finland

Abstract

The coolant outlet temperature in VVER-440 type nuclear reactors is measured using thermocouples. In the Loviisa nuclear power plant, the thermocouple readings are used in the evaluation of the fuel assembly power. The assembly power is needed as an input for the reactor core performance monitoring system. However, since the coolant is not perfectly mixed in the assembly head, the thermocouple reading might differ from the real average temperature of the flow in the fuel assembly. In order to study the coolant mixing in the fuel assembly head, a 3D computational fluid dynamics (CFD) analysis is conducted. The CFD model describes the head parts of the fuel assembly, including the ends of the fuel rods, a central tube, a top flow plate, lifting bars, a catcher and the thermocouple. The computation grid is a tetrahedral and hexahedral hybrid mesh consisting of 22 - 32.5 million cells. Following The Best Practice Guidelines, the model's sensitivity to boundary conditions, turbulence models and grid resolution is assessed. The CFD analysis provides information on the coolant mixing in the assembly head and thereby helps to define the average coolant outlet temperature from the thermocouple reading.

1. INTRODUCTION

In the Loviisa nuclear power plant, a VVER-440 type nuclear reactor, the coolant outlet temperature is measured using thermocouples. The thermocouples are placed above 190 of the total 313 fuel assemblies, depicted in Figure 1, and the temperature readings are used in the evaluation of the enthalpy rise of the coolant in the reactor. The thermocouple readings are processed in the reactor core performance monitoring system, RESU (Antila, 1999), which monitors the performance of the reactor in order to insure safe operation. Knowing the mass flow and the temperature of the coolant entering the fuel assembly, RESU interprets the thermocouple reading into enthalpy rise of the coolant. The result is used in adjusting the power distribution obtained from the theoretical neutron flux calculation.

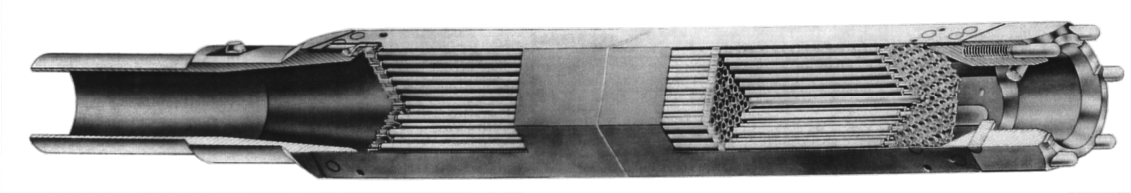

Fig. 1: A VVER-440 type fuel assembly. The length is reduced in the picture. The flow direction is from down to up (from left to right in the figure).

The coolant, flowing upwards through the fuel assembly, is heated by the fuel rods. The fuel rods have different powers and therefore the temperature field of the coolant at the rod bundle outlet is not homogeneous. Since the mixing of the coolant in the fuel assembly head part is not perfect, the thermocouple might not register the average coolant temperature but a slightly higher or a slightly lower reading.

In order to study the mixing of the coolant in the assembly head, a 3D computational fluid dynamics (CFD) model is created. The goal is to predict the thermocouple reading for different coolant temperature distributions at the fuel rod bundle outlet.

Previous work regarding the CFD simulation of the fuel assembly head has been done in Fortum Nuclear Services Ltd in 1999 - 2004 (Toppila, 2004). Mixing of the returning bypass flow (the coolant flowing in the gap between assemblies and returning through holes in the shroud box) was studied both by CFD methods and experimentally. In the experiments, a full-scale assembly model at room temperature was used. CFD models were created for all fuel assembly geometries used at the Loviisa power plant at that time. The models contained $3x10^5$ - $9x10^5$ cells. The effect of the central tube flow and different central tube geometries was also studied using CFD. In addition to the fuel assembly head studies, the flow in the fuel rod bundle has been modelled using CFD in (Brandt, 2009a,b) and (Lestinen, 1999). Boundary conditions for the fuel assembly head model can be obtained from the fuel rod bundle calculations.

Similar CFD studies regarding the coolant mixing in the head parts of the VVER-440 type fuel assembly have also been conducted by (Tóth, 2008, 2009), confirming the incomplete mixing of the coolant and the deviation in the thermocouple reading compared to the real average temperature.

2. CASE DESCRIPTION

The coolant, leaving the rod bundle, enters the assembly head with a mass flow rate of about 24 kg/s. The shroud box surrounding the fuel rods is of hexagonal shape. The shroud box defines the coolant and thus prevents it from mixing with the neighbouring fuel assemblies. The coolant flows through the top flow plate, past the catcher and the thermocouple, and through the channel in the upper core support plate.

The Reynolds number at the rod bundle outlet is about 300 000, based on the average velocity and the hydraulic diameter, and the flow is fully turbulent. A mass flow of about 0.12 kg/s enters the central tube on the same level as the main inlet. The Reynolds number of the flow in the central tube is about 200 000. A bypass flow of about 1.4 kg/s enters through the twelve bypass inlets, with a Re-number of about 150 000.

The CFD model, depicted in Figure 2, contains the ends of the fuel rods, a central tube, twelve bypass flow inlets, a top flow plate, two lifting bars, a catcher and the thermocouple.

In the radial direction, the main inlet is divided in 7 sections with the shape of rings, each of which is the inlet for a different species of water. The inlet sections are depicted in Figure 2. The species have same material properties and they are named species 1 - species 7 at the main inlet, species 8 at the central tube and species 9 at the bypass inlets. The division of the coolant fluid, water, into different species allows monitoring of the mass fraction of species at the thermocouple. The mass fractions can be further used for defining the thermocouple reading for different coolant temperature distributions at the rod bundle outlet.

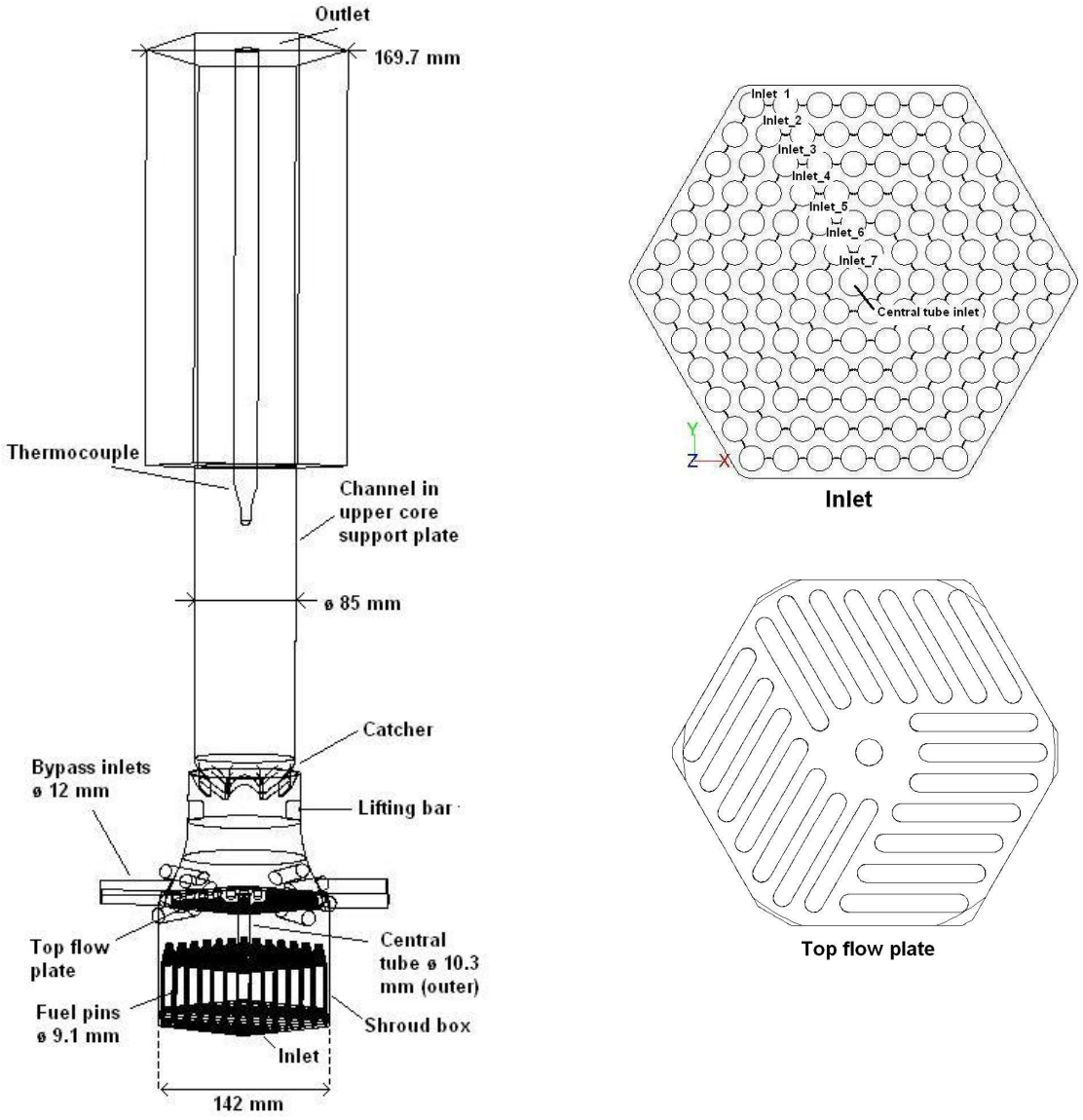

Fig. 2: CFD model of fuel assembly head. The outlines of the model are shown on the left, together with some measures. On the right, upper figure, the division of the inlet is presented. The lower figure on the right represents the top flow plate.

The case is modelled using ANSYS FLUENT 12.0 software and the computational grid is generated with ANSYS Gambit 2.4.6. The simulations were run on a 64-bit Linux workstation with Intel Xeon X5482 @ 3.20 GHz processor. Parallel simulation with 4 cores took about 250 hours of wall clock time for the base mesh and about 400 hours for the fine mesh.

3. CFD MODEL DESCRIPTION

3.1 Geometry

The geometry is created based on original drawings of the fuel assembly head. Some minor modifications were made to the geometry. The wedge, which is formed on the outer periphery around the catcher, is made somewhat less sharp in order to facilitate meshing.

3.2 Grid

The computational grid, shown in Figure 3, is a hybrid mesh consisting of both hexahedral and tetrahedral cells. Due to the complexity of the geometry, the bypass inlets and a zone 30 mm above and 40 mm below the top flow plate are meshed using tetrahedral cells. The rest of the model is meshed using hexahedral cells. In order for turbulence model wall functions to work properly, the aim was to have a few cells in the log-law layer and keep wall $y+$ values between 30 - 300, although this was not achieved in all parts of the model. Two grids with different resolutions were made for testing the grid independency of the solution. Due to computational capacity restrictions, the grid resolution could not be doubled throughout the entire flow field. Therefore, adaption was performed only on the flow path of one species of water. The species chosen was species 7, which represents the mass flow of inlet 7. The adaption was performed in areas where the mass fraction of species 7 was in the range of 0.06 to 1. The volume contained 1.5×10^6 cells. Each of these cells was divided in eight, thus augmenting the size of the computational grid by 10.5×10^6 cells. The adaption was done using the automatic adaption tool of ANSYS FLUENT. Information of the computational grid is listed in Table 1.

Table 1: List of computational grids.

Computational grid	Number of cells	Average cell size [m^3]	Max cell size [m^3]	Min cell size [m^3]	% of wall bound cells with $30 \leq y+ \leq 300$	Adaptions
Base mesh	22×10^6	1.1×10^{-8}	5.1×10^{-8}	7.1×10^{-14}	92.5 %	-
Fine mesh	32.5×10^6	1.1×10^{-8}	5.1×10^{-8}	2.1×10^{-14}	93.5 %	Adaption on the flow path of species 7

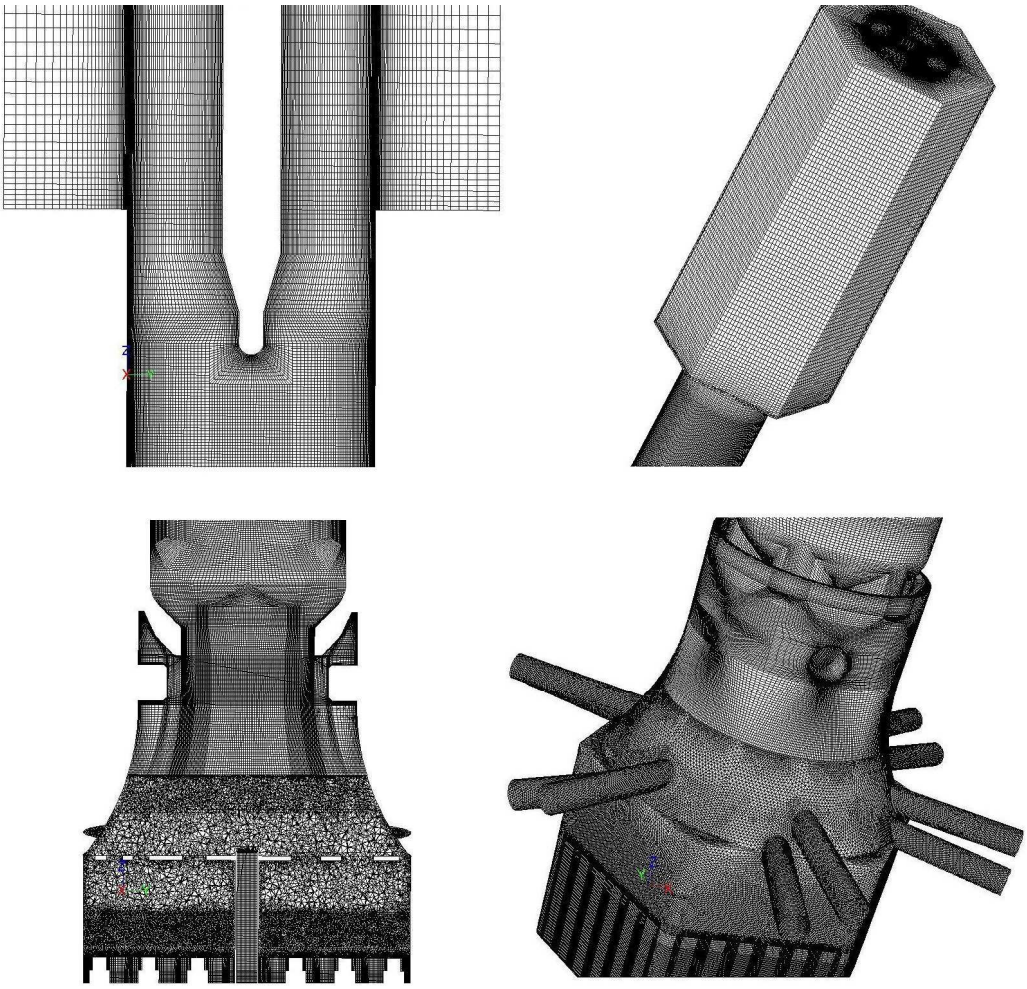

Fig. 3: Computational grid (basic mesh). The two upper figures represent the upper part of the mesh, a cutaway figure on the left and the surface mesh on the right. The lower figures represent the lower part of the mesh with a cutaway view on the left and the surface mesh on the right.

3.3 Physical and numerical models

The equations for conservation of mass and momentum are solved, Eq. (1) and (2). The local mass fraction of each species, Y_i, is predicted by solving a convection-diffusion equation, Eq. (3). The mass diffusion in turbulent flow is computed according to Eq. (4). The turbulent Schmidt number, defined in Eq. (5), is involved in the computation of the turbulent mass diffusion of species. The mass diffusion of turbulent flows is more effective than the mass diffusion of laminar flows. The turbulent Schmidt number is used to convert the turbulent viscosity into turbulent diffusion.

When needed, the energy equation is solved for, as well. For turbulence modelling, the standard κ-ε turbulence model (Launder, 1972) with standard wall functions was used. The κ-ω turbulence model (Wilcox, 1998) was tested, as well.

$$\frac{\partial \rho}{\partial t} + \nabla \cdot (\rho \vec{v}) = 0 \qquad (1)$$

$$\frac{\partial}{\partial t}(\rho\vec{v}) + \nabla \cdot (\rho\vec{v}\vec{v}) = -\nabla p + \nabla \cdot (\bar{\bar{\tau}}) \quad (2)$$

$$\frac{\partial}{\partial t}(\rho Y_i) + \nabla \cdot (\rho\vec{v} Y_i) = -\nabla \cdot \vec{J}_i \quad (3)$$

$$\vec{J}_i = -(\rho D_{i,m} + \frac{\mu_t}{Sc_t})\nabla Y_i \quad (4)$$

$$Sc_t = \frac{\mu_t}{\rho D_t} \quad (5)$$

In Eq. (1) and (2), ρ is the density [kg/m^3], $\vec{v}$ is the velocity [m/s], p is the pressure [Pa] and $\bar{\bar{\tau}}$ is a stress tensor. In Eq. (3), $\vec{J}_i$ is the turbulent mass diffusion, defined in Eq. (4). In Eq. (4), $D_{i,m}$ is the mass diffusion coefficient for species i in the mixture, μ_t is the turbulent viscosity, Sc_t is the turbulent Schmidt number, defined in Eq. (5). D_t is the turbulent diffusivity.

The standard pressure-based solver of ANSYS FLUENT is used. For pressure-velocity coupling, the SIMPLE scheme is used. Second-order upwind spatial discretization is used for momentum, turbulence, species transport and the energy equation.

3.4 Boundary conditions

The boundary condition values are chosen to correspond to the real plant parameters of Loviisa NPP. The main inlet of the CFD model is divided in seven sections, inlet 1 - inlet 7, as depicted in Figure 2. For each inlet, a different species of fluid is used. The fluids are named water 1 - water 9 and they have equal material properties. Water 1 is used in inlet 1 and so on. Water 8 is used for the central tube inlet and water 9 is used in the bypass inlets. For the main inlet boundary, a velocity of 3.659 m/s is used. The central tube inlet is a mass flow inlet of 0.12 kg/s, which corresponds to a velocity of 2.8 m/s. The bypass inlets have a total mass flow of 1.36 kg/s, which corresponds to a velocity of 1.4 m/s. Both inlets have the same turbulence values as the main inlet. The walls are treated as adiabatic walls with no slip boundary condition. The space after the upper core support plate channel, before the outlet, is treated as symmetry boundaries. The outlet is a pressure outlet with a gauge pressure of 0 Pa and backflow turbulence values are the same as the inlet values. The backflow mass fraction is set to 0.1 for each species.

The bypass inlets consist of 12 holes in the shroud box. In order to minimize the disturbance caused by the boundary, the bypass inlets were extended further away, see Figures 2 and 3.

Since experimental results are not available, the turbulence quantities are approximated. The turbulence values were given as turbulent intensity I = 2% and the hydraulic diameter D_h = 0.01 m at the main inlet. For the bypass and central tube inlets the values were given as turbulent kinetic energy, $\kappa = 1\text{x}10^{-4}$ m^2/s^2 and for turbulent dissipation rate $\varepsilon = 1\text{x}10^{-5}$ m^2/s^3. Sensitivity studies are performed, as recommended by the Best Practice Guidelines. As a sensitivity study, the turbulence values from the fuel rod bundle model (Brandt, 2009) are used. The values were $\kappa = 8\text{x}10^{-3}$ - $9\text{x}10^{-2}$ m^2/s^2, ε = 0.3 - 132 m^2/s^3 and I = 7.2 - 25 %.

3.5 Material properties

The average temperature of the water is 302.9 °C and the pressure is 123 bar. All nine species created have equal material properties, a constant density of 714 kg/m^3 and a viscosity of $1\text{x}10^{-4}$ kg/ms. When the energy equation is enabled, the material properties are given as a temperature dependent piecewise linear function including eleven points. The material properties were taken from the NIST Standard Reference Database (Lemmon, 2010).

4. CALCULATIONS

A reference case, corresponding as closely as possible to real plant parameters, was first simulated as steady state using both the base mesh and the fine mesh. Sensitivity studies for boundary conditions and turbulence models, and numerical studies for grid independency and convergence criterion were performed on the reference case. Convergence was monitored by plotting residuals and selected target values. The target variables chosen were the mass fraction of species 2, species 5 and species 7 at the thermocouple, velocity magnitudes at two different points and the static pressure at inlet 7. The velocity points, a and b, were located in two important areas where mixing occurs, above the top flow plate and above the core catcher. The most important target values are the mass fractions of different species at the thermocouple housing, since determining them was the main goal of the simulation. The influence of different inlet sections at the thermocouple can be studied using a variable β, called the "weight factor". The variable β works as either a gain factor or a damping factor, telling how much a certain inlet affects the outcome of the thermocouple reading. If the coolant was perfectly mixed, the weight factor would be 1 for each inlet section. Since this is not the case in reality, some inlet sections will have a weight factor larger than 1 and some less than 1. A weight factor larger than 1 indicates that the mass flow from the inlet section is strongly present at the thermocouple and vice versa. The weight factor is defined as the mass fraction of a certain species at the thermocouple, divided by the mass fraction of the same species at all inlets. In equation form, the weight factor can be written as

$$\beta_i = \frac{\alpha_{i,tc}}{\alpha_i} \tag{6}$$

where $\alpha_{i,tc}$ is the mass fraction of species i at the thermocouple housing and α_i is the mass fraction of species i at the inlets. Mass fraction is defined as the mass flow [kg/s] of a species divided by the total mass flow [kg/s] of all species.

When the weight factors are determined for a reference case, one can use them to calculate an estimate for the thermocouple readings for another coolant temperature distribution at the rod bundle outlet. The estimated thermocouple temperature is written as

$$T_{TC,est} = \frac{1}{\sum_i (\beta_i^{ref} \alpha_i)} \sum_i (\beta_i^{ref} \alpha_i T_i) \tag{7}$$

where β_i^{ref} is the reference case β-value for inlet i and T_i is the average temperature of inlet i.

Determining the weight factors by using a CFD model gives a possibility to implement them in the RESU system, if needed.

4.1 Numerical studies

Case 1 represents the reference case. For monitoring convergence, the approach of the Best Practice Guidelines (Casey, 2000) was used. The mass imbalance of the flow field was monitored together with the target values. The sum of the absolute values of the mass imbalance in the flow field was plotted. Mesh sensitivity was studied in Case 3 by using the finer mesh. The values of the target values give some information on the grid independency of the result. If the values remain unchanged after the adaption, it indicates that the mesh resolution is sufficient to produce an accurate result. Of course, adapting on the path of species 7 mostly confirms the grid accuracy in this particular area. However, due to restrictions in computational resources, adaption of the whole flow area was not possible. The uncertainty due to the grid convergence can be described via the grid convergence index (GCI), (Roache, 2009). The GCI is a measure of the percentage the computed value is away from the value of the asymptotic numerical value. For a case with two meshes, the GCI for the fine grid is presented in Eq. (8) and for the coarse grid in Eq. (9).

$$\text{GCI [fine grid]} = F_S \left| \frac{\Theta_1 - \Theta_2}{\Theta_1} \right| \frac{1}{r^p - 1} \quad (8)$$

$$\text{GCI [coarse grid]} = r^p \,\text{GCI [fine grid]} \quad (9)$$

The term F_S is a factor of safety, in this case $F_S = 3$, as recommended in (Roache, 2009), since it is not confirmed that the grids are in the asymptotic region and only two grids are available in stead of three. Θ is the target value, index one indicating the finer mesh and index two the coarser mesh. r is the mesh refinement ratio and p is the truncation error order of the discretization scheme. In the ideal case, for a second order discreatization scheme, p would equal to 2. The cases for numerical studies are shown in Table 2.

4.2 Sensitivity studies and simulation case

The turbulence model is assessed by using both the κ-ε and κ-ω turbulence models. The κ-ω turbulence model is tested in Case 2. The sensitivity for the central tube inlet boundary was studied in Case 4 by using a mass flow rate value based on previous CFD studies of the central tube for the mass flow rate. Sensitivity studies for the boundary conditions are performed by using the data from the fuel bundle model (Brandt, 2009) in Case 5. In Case 6, the turbulent Schmidt number is changed from the default value of $Sc_t = 0.7$ to $Sc_t = 0.85$.

Case 7 is simulated using a temperature profile from RESU calculations at the inlet. The energy equation is solved during the simulation, thus allowing temperature readings of the thermocouple to be monitored. The temperature readings are then compared to the "weight factor" approach. A matrix for sensitivity studies is shown in Table 2.

Table 2: Case matrix for numerical studies, sensitivity studies and simulation case. Varied parameters are printed as bold.

Case	Mesh	Turbulence model	Turbulence model inlet values	Main inlet boundary, v [m/s]	Central tube inlet boundary, $\dot{m}$ [kg/s]	Bypass flow inlet boundary, $\dot{m}$ [kg/s]	Energy eq. solved
1	Base mesh	κ-ε standard wall functions	I = 2 %, Dh = 0.01 m	3.659	0.12	1.36	-
2	Base mesh	**κ-ω standard wall functions**	I = 2 %, Dh = 0.01 m	3.659	0.12	1.36	-
3	**Fine mesh**	κ-ε standard wall functions	I = 2 %, Dh = 0.01 m	3.659	0.12	1.36	-
4	Base mesh	κ-ε standard wall functions	I = 2 %, D_h = 0.01 m	3.659	**0.3192 (best estimate)**	1.36	-
5	Base mesh	κ-ε standard wall functions	**κ and ε profiles from fuel rod bundle CFD model**	**Velocity profile from fuel bundle CFD model**	0.12	1.36	-
6	Base mesh	κ-ε standard wall functions, **Sc_t = 0.85**	I = 2 %, D_h = 0.01 m	3.659	0.12	1.36	-
7	Base mesh	κ-ε standard wall functions	I = 2 %, D_h = 0.01 m	3.659, **temperature profile from RESU calculation**	0.12	1.36	yes

5. RESULTS

5.1 Numerical studies

The cases seemed to approach a converged solution. However, instead of settling to a final value, the target variables seemed to oscillate. The value, around which the oscillation occurred, was then approximated as the final value. Oscillation may be a sign of time dependent behaviour. In order to improve convergence, the under-relaxation factors were reduced. The pressure under-relaxation was reduced from 0.3 to 0.2, turbulent kinetic energy and dissipation rate from 0.8 to 0.7 and turbulent viscosity from 1 to 0.7. The sum of the absolute value of the mass imbalance over all cells in the computational grid was monitored during simulation.

Figure 4 shows the mass imbalance as a function of iterations in Case 1. The mass imbalance decreases rapidly during the first 1000 iterations, after which it steadily settles to a value of about $2x10^{-3}$ kg/s.

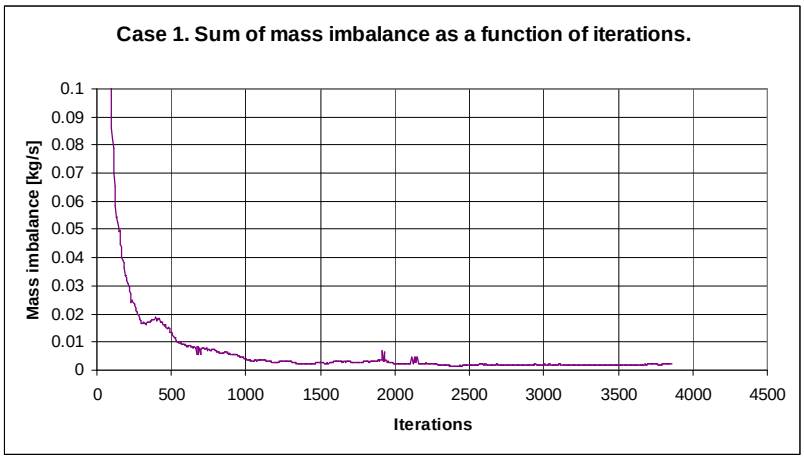

Fig. 4: The sum of the absolute values of mass imbalance over all cells as a function of iterations in Case 1.

The target values also seem to settle to their final value after about 1000 iterations. Figure 5 shows the mass fraction of species 7 at the thermocouple housing as a function of iterations.

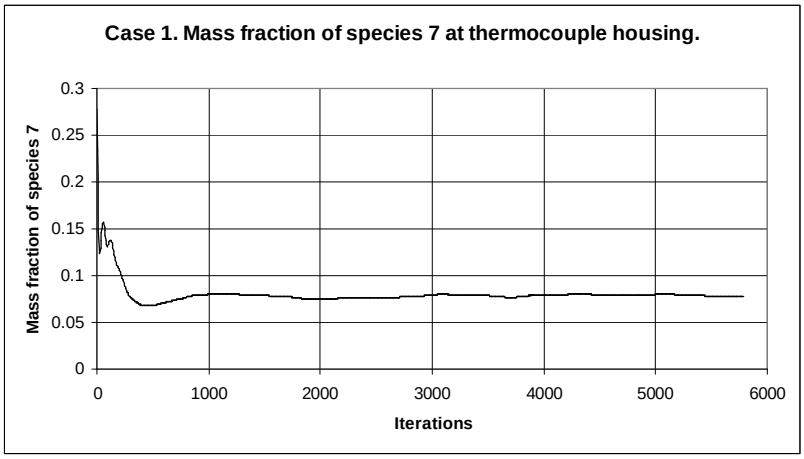

Fig. 5: Mass fraction of species 7 at the thermocouple housing as a function of iterations.

Figure 6 shows the mass fraction of species 7 as a function of the mass residual. The target value does not change very much after the mass balance has decreased below $6x10^{-3}$ kg/s. Figure 6 illustrates the level of mass residual after which the case has reached the maximum achievable accuracy.

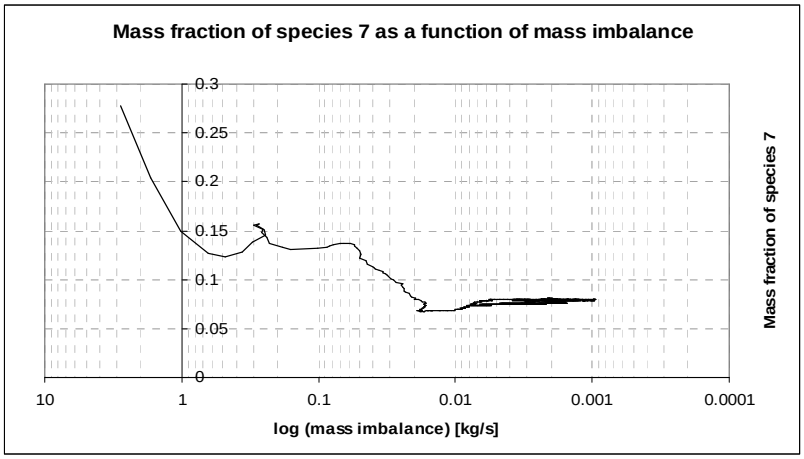

Fig. 6: Mass fraction of species 7 at the thermocouple as a function of mass residual.

The results of the numerical studies are shown in Table 3. The interesting target value in Case 3 is the mass fraction of species 7, since the mesh was adapted based on the concentration of this species in the flow field. The increase in mesh resolution shows a 1 % change in the mass fraction.

The grid convergence index for the fine mesh, Eq. (8), and the coarse mesh, Eq. (9) was calculated using Case 3 as fine mesh and Case 1 as coarse mesh. The target value used was the mass fraction of species 7 at the thermocouple housing. The grid refinement ratio is approximated to be 2, since the grid resolution is doubled on the flow path of species 7. For the truncation error of the discretization scheme, p, the values 2 and 1.5 are tested. Using these values, the GCI [fine grid] is 1.3% and 2%, and the GCI [coarse grid] is 5% and 6%. These GCI values are fairly small, considering that the factor of safety used is conservative, $F_S = 3$, thus providing confidence that the solution is not very far from the asymptotic value.

The results of the target value monitoring and GCI index indicate that the mesh resolution in the base mesh is sufficient and an increase of mesh resolution would not significantly improve accuracy of the solution.

Figure 7 shows the β- values, Eq. (6), for Case 1. It can be seen clearly that the inlets closest to the middle of the fuel assembly, and thereby closest to the thermocouple, have the largest weight on the thermocouple reading, compared to the mass fraction at inlet.

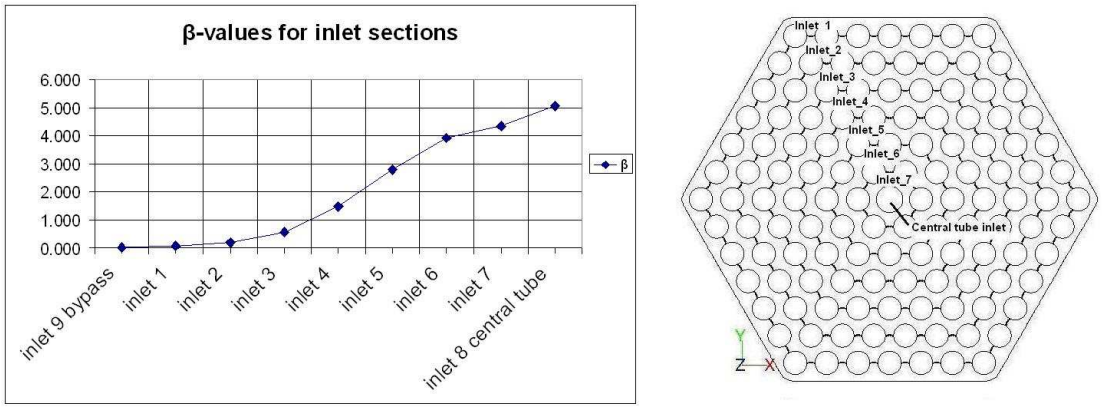

Fig. 7: β -values for Case 1.

5.2 Sensitivity studies and simulation case

The κ-ω turbulence model was tested in Case 2. The differences in the mass fractions compared to Case 1, with the κ-ε turbulence model, were about 0.4 % - 11 %. The difference of species 7 mass fraction was about 9 %, and while the GCI [coarse grid] was 5 % it is clear that the turbulence model affects the results. Which model is better cannot be justified based on simulation of this study, but would require e.g. comparison with some experimental data.

The static pressure and velocities at points a and b differ in Case 5 since a different velocity profile was used at the inlet. However, the mass fractions are similar to the other cases; the differences in mass fractions compared to the reference case are 0.7 - 2 %. The change of boundary conditions for the central tube in Case 4 did not have a large effect on the results. The mass fractions differed 1 - 3 % compared to the reference case. The results of the target values are given in Table 3.

The turbulent Schmidt number was altered in Case 6, which resulted in 2 - 16 % changes in the mass fractions compared to the reference case. While the difference is this large, it is clear that the turbulent Schmidt and Prandtl numbers should be carefully chosen.

In Case 7, a temperature profile from RESU was used at the inlet. The thermocouple temperature given by Fluent was then compared to the temperature given by weight factor calculations. An estimate for the thermocouple reading is formed, using Eq. (7). For Case 7, the estimate was 312.404 °C, using Case 1 as reference case. The thermocouple temperature given by Fluent was 312.418 °C. The estimate is therefore very accurate. Should the coolant be perfectly mixed, the thermocouple would register the average temperature of the fuel rod bundle outlet, which in Case 7 is 308.572 °C. The deviation between the thermocouple reading and the real average temperature is 3.8 °C. The results of (Tóth, 2008 and 2009) were of the same order of magnitude, with maximum deviations of about -2.6 °C, even though the cases studied in (Tóth, 2008 and 2009) are not identical to the cases presented in this paper.

The last row in Table 3 reports the result from earlier work (Toppila, 2004). Though a different computation grid, containing about $3x10^5$ - $9x10^5$ cells, and different boundary conditions were used, the results are somewhat similar.

Table 3: Results for sensitivity studies and simulation case.

Case	Mass fraction of species 2 at thermocouple	Mass fraction of species 5 at thermocouple	Mass fraction of species 7 at thermocouple	Static pressure at inlet 7 [Pa]	Velocity magnitude at point *a* [m/s]	Velocity magnitude at point *b* [m/s]
1	0.044	0.283	0.080	22700	9.44	3.99
2	0.039	0.282	0.087	23300	9.47	3.90
3	0.045	0.281	0.079	22700	9.44	4.00
4	0.043	0.273	0.079	23000	9.49	3.99
5	0.043	0.285	0.080	15700	7.80	3.15
6	0.037	0.289	0.088	22700	9.44	3.99
7	0.040	0.280	0.081	22500	9.67	3.56
Previous studies (2004)	-	0.3	0.05	-	-	-

6. SUMMARY

A CFD model of the head parts of a VVER-440 type fuel assembly was created. The aim was to study the coolant mixing in the fuel assembly head, and to predict the reading of thermocouples located in the fuel assembly heads. The thermocouple reading depends on the temperature distribution of the coolant at the fuel rod bundle outlet and on the mixing before the thermocouple. In the ideal case, the coolant would be perfectly mixed and the thermocouple would register the average temperature. In reality, the coolant is not perfectly mixed and there will be a small deviation between the real average temperature of the coolant and the temperature registered by the thermocouple.

The CFD model contains the ends of the fuel rods, surrounded by the shroud box, the central tube, the top flow plate, bypass inlets, lifting bars, the catcher and the thermocouple. The model outlet is placed beyond the upper core support plate of the reactor. The computational grid is a hybrid tetrahedral and hexahedral mesh containing 22 - 32.5 million cells. A reference case was first calculated, using boundary conditions that correspond to real plant parameters. Sensitivity studies for mesh resolution, turbulence model and boundary conditions were conducted on the reference case. Convergence was monitored by plotting target values and residuals. A solution approaching convergence was found, however, the case showed signs of what might be time dependent behavior. The case was not very sensitive for changes in the boundary conditions or mesh resolution. The case was more sensitive to the turbulence model and altering of the turbulent Schmidt number, showing up to 11% and 16% differences in target values compared to the reference case.

Weight factors, denoted as the β variables, were determined for the reference case. The weight factors were then used for estimating the thermocouple reading for another case with a given temperature distribution. The estimate was very similar compared to the value given by the CFD simulation with the energy equation solved.

REFERENCES

ANSYS FLUENT 12.0 User's Guide, ANSYS, Inc. 2009-01-29

M. Antila, J. Kuusisto, "Recent Improvements in On-line Core Supervision at Loviisa NPP", *OECD/NEA Workshop on Core Monitoring for Commercial Reactors*, Stockholm, Sweden, 4- 5 October 1999

T. Brandt, T. Lahtinen, T. Toppila, "CFD Study on Coolant Mixing Inside VVER-440 Fuel Rod Bundle", In *Proc of 19th Symposium of AER on VVER Reactor Physics and Reactor Safety*, St. Constantine and Elena resort, Varna, Bulgaria, 21 – 25 September, 2009a.

T. Brandt, T. Toppila, "CFD study on mixing in VVER-440 fuel rod bundle with guiding vanes in spacer grids", In *Proc of 17th International Conference on Nuclear Engineering (ICONE -17)*, Brussels, Belgium, 12-16 July, 2009b.

M. Casey, T. Wintergerste (ed.), *Best Practice Guidelines*, Version 1.0. ERCOFTAC Report, 2000.

B. E. Launder, D. B. Spalding, *Lectures in Mathematical Models of Turbulence*, Academic Press, London, England, 1972.

E.W. Lemmon, M.O. McLinden, D.G. Friend, "Thermophysical Properties of Fluid Systems" in *NIST Chemistry WebBook, NIST Standard Reference Database Number 69***,** Eds. P.J. Linstrom and W.G. Mallard, National Institute of Standards and Technology, Gaithersburg MD, 20899, http://webbook.nist.gov, (retrieved April 15, 2010).

V. Lestinen, P. Gango, "Experimental and Numerical Studies of the Flow Field Characteristics of VVER-440 Fuel Assembly" *In 9th International Topical Meeting on Nuclear Reactor Thermal Hydraulics (NURETH-9)*, San Francisco, USA, 3 - 9 October, 1999.

J. Mahaffy, B. Chung, F. Dubois, F. Ducros, E. Graffard, M. Heitsch, M. Henriksson, E. Komen, F. Moretti, T. Morii, P. Mühlbauer, U. Rohde, M. Scheuerer, B. L. Smith, C. Song, T. Watanabe, G. Zigh, *Best Practice Guidelines for the use of CFD in Nuclear Reactor Safety Applications*, Nuclear Energy Agency, Report NEA/CSNI/R(2007)5, 15 May 2007.

P. J. Roache, *Fundamentals of Verification and Validation*, Hermosa Publishers, Socorro, New Mexico, USA, 2009.

S. Tóth, A. Aszódi, "CFD Study on Coolant Mixing in VVER-440 Fuel Rod Bundles and Fuel Assembly Heads", *XCFD4NRS Experiments and CFD Code Applications to Nuclear Reactor Safety, OECD/NEA & IAEA Workshop*, Grenoble, France, 10 - 12 September 2008.

S. Tóth, A. Aszódi, "Determination of Weight Factors for VVER-440 Fuel Assemblies with Burnable Poison", *19th Symposium of AER on VVER Reactor Physics and Reactor Safety*, St. Constantine and Elena Resort, Varna, Bulgaria, 21 - 25 September 2009.

T. Toppila, V. Lestinen, "CFD Simulation of Coolant Mixing Inside the Fuel Assembly Top Nozzle and Core Exit Channel of a VVER-440 Reactor", *14th Symposium of AER on VVER Reactor Physics and Reactor Safety*, Espoo, Finland & Baltic Sea Cruise to Stockholm, 13 - 17 September 2004.

D. C. Wilcox, *Turbulence Modeling for CFD*, DCW Industries, Inc., La Canada, California, 1998.